PCCP

Accepted Manuscript

ROYAL SOCIETY OF CHEMISTRY

www.rsc.org/pccp

Concentration dependence of the up- and down-conversion emission colour of Er^{3+}-doped Y_2O_3; a time-resolved spectroscopy analysis

Haizhou Lu[a], William P. Gillin[a,b]* and Ignacio Hernández[c]*

[a] School of Physics and Astronomy, Queen Mary University of London, Mile End Road, London, E1 4NS, UK

[b] College of Physical Science and Technology, Sichuan University, Chengdu, 610064, People's Republic of China

[c] Dpto. CITIMAC, Universidad de Cantabria, Facultad de Ciencias, Avda. Los Castros, s/n 39005, Santander, Spain

Abstract

In this paper, a series of Er^{3+}-doped Y_2O_3 samples are systematically investigated, focusing on the effect of the doping concentration on the emission lifetime and spectrum under both 488 nm and 980 nm excitations. Decay times of the $^4S_{3/2}$ and $^4F_{9/2}$ emitting states under 488 nm and 980 nm excitations are found to be different and concentration dependent. We explain these variations in terms of the changes in the up-conversion routes caused by the predominance of energy exchanges that involve the lowest lying excited states.

Introduction

Lanthanide doped up-conversion (UC) materials, which can convert infrared radiation into visible luminescence via excited state absorption (ESA) or energy transfer (ET) to excited states, have been widely investigated since their discovery in the 1960s [1-3]. Lanthanide doped UC materials can be used for a variety of applications [2], ranging from biology to solar conversion; the narrow visible emission excited by low energy can be employed in biomedicine [4], solid state laser [5] and illumination [6], and the materials can be implemented in a functional phosphor layer to improve the efficiency of solar cell by means of converting infrared light, which cannot be absorbed by solar cell, into absorbable visible light [7-8].

Although the energy of the excitation and emission bands, due to optical transitions within the $4f^n$ energy manifolds, are weakly dependent on the lanthanide ion's surroundings, changes in the host matrix may affect the emission intensity as well as the UC routes. Lanthanide based UC halides [6-7, 9-18], glasses [19-21] and oxides [8, 22-38] have been studied both for a basic understanding of the underlying physics and for a number of applications. However, it has been a challenge to find the most chemically stable and efficient material. β-$NaYF_4$ is one of the most studied materials [6-7, 9-15], as it yields one of the highest UC efficiency [37]. However, it requires a relatively complex synthesis method to make pure (thermally instable) β-$NaYF_4$, which makes it more expensive and less practical for industrial applications [25]. On the contrary, Y_2O_3 has an excellent stability [27] and the synthesis is simple. Y_2O_3 also has a low phonon energy (430-550 cm^{-1}), which makes it a suitable and practical prototype UC material [32]. Er^{3+}-doped Y_2O_3 UC systems have been previously investigated [22-24, 29-34]. These studies were presided by a twofold objective: to understand the UC mechanisms upon different excitation wavelengths and the changes in light emission colour upon changes in the erbium concentration or excitation. However, current understanding still involves an ambiguous combination of cross relaxation (CR) processes (two-ion energy transfer involving excited states) and UC routes.

The UC emission colour (that is, the ratio between the different emission bands) as a function of composition is a phenomenon of high interest, as it should allow the material use for multicolour applications. J. A. Capobianco *et al.* reported that the green to red ratio decreases via UC at an excitation wavelength of 815 nm with increasing erbium concentration in Er^{3+}-doped Y_2O_3 system. The change was explained by the occurrence of CR via: $[^4I_{9/2}, {}^4I_{11/2}] \rightarrow [^4I_{13/2}, {}^4F_{9/2}]$ [23]. However, the difference of emission spectra under short excitation wavelength (488 nm) and UC pumping (815 nm) cannot be explained by this mechanism only. The same group postulated that the CR process: $[^4F_{7/2}, {}^4I_{11/2}] \rightarrow [^4F_{9/2}, {}^4F_{9/2}]$ populates the red-emitting state by depopulating the green ones with UC pumping (980 nm) [24] causing a systematic difference of emission spectra under 488 nm and 980 nm excitations. However, this CR process happens under both 488 nm and 980 nm excitations, thus the theory is not enough to explain the spectrum difference. We believe that these incomplete models need further testing, clarification and refinement through the insight provided by the population and de-population dynamics. It is also worth noting that despite the great activity and interest in co-doped systems with ytterbium sensitizer and erbium emitters, the green to red ratio changes observed with varying both erbium and ytterbium concentrations are still the subject of major revisions [14, 38]: recently, R. B. Anderson *et al.* reported that the red emission is due to a three photon process in Yb/Er co-doped β-$NaYF_4$ system under 1 μm excitation, involving CR within Er ions from higher-lying states [15]. The need for accounting for all the processes and the indefinition of those which are important is in part due to the lack of dynamic data and the difficulty in modelling so many states and ions. Therefore, we expect our work in the simpler Er^{3+}-doped Y_2O_3 system to contribute to understanding more practical systems, such as the Yb/Er co-doped material.

In order to fully understand the UC mechanism and emission colour change, and give some fundamental information for co-doped systems, we have performed a study of the Er^{3+}-doped Y_2O_3 system using time resolved spectroscopy, which allows the recording of each emitting state's time decay profile and is a method to understand the character of the emitting states [25]. The decay times of the emitting states offer the possibility to quantify not only the probability of radiative processes but, importantly, that for non-radiative processes such as CR, which are critical to determine dynamical processes and colour properties of optical materials. Moreover, information can be obtained on the populating mechanisms. To the best of our knowledge, there has been no such a systematic study of the $^4I_{11/2}$ and $^4I_{13/2}$ lifetimes in Y_2O_3 under both 488 nm and 980 nm excitations [19-21, 30-32], which are vital to understand UC processes in this material and in co-doped systems [8, 14, 15, 25, 38].

Experimental

Synthesis of Er^{3+}-doped Y_2O_3 materials

$Y(NO_3)_3{\cdot}6H_2O$ (99.98%) and $Er(NO_3)_3{\cdot}6H_2O$ (99.98%) were purchased from Alfa Aesar. Er^{3+}-doped Y_2O_3 was synthesized through a conventional spray pyrolysis technique. Typically, a mixture of (1-*x*) M $Y(NO_3)_3{\cdot}6H_2O$ and *x* M $Er(NO_3)_3{\cdot}6H_2O$ was dissolved in 50 ml de-ionized water. The solution was sprayed, using a conventional spray gun, onto a piece of glass, which was heated to 450 °C on a hotplate creating a uniformly distributed white powder film of Er^{3+}-doped Y_2O_3. The white film was then removed and annealed in a furnace at 1000 °C for 2 hours to produce moisture-free material. A systematic lifetime study under different annealing temperatures and time is given in the supplemental information (SI), which shows the optimum annealing conditions.

Instrumentation

Powder X-ray diffraction (XRD) patterns of the dried powders were recorded using Cu Kα radiation (λ=1.5418 Å). The erbium doping concentration was confirmed by energy dispersive X-ray spectroscopy (EDX) at an accelerating voltage of 20 kV.

For the down-conversion (DC) lifetime and spectral measurements, a Continuum Panther optical parametric oscillator (OPO) was used to provide ~7 ns pulse with a typical power density of 3×10^6 W/cm^2 at a wavelength of 488 nm. Also, a 405 nm continuous wave (CW) laser (VL01132A02) with a power density of 16 W/cm^2, which is modulated by a digital pulse wave generator, was used to investigate the pulse length effect. The fluorescence was dispersed in a Triax 550 spectrometer (gratings: 1200 and 600 lines/mm) and detected by a Hamamatsu R5509-72 photomultiplier.

For the UC lifetime measurement, a 980 nm CW diode laser with a maximum power density of 50 W/cm^2 was used, which was modulated by a digital square wave generator at a frequency of 11 Hz. The excitation laser was removed from the fluorescence using a short pass filter (10SWF-950-B) which was dispersed and collected using the same system as for the DC measurements.

Results and discussion

Structural characterization

The as synthesised Er^{3+}-doped Y_2O_3 is a pure single cubic phase [35]. XRD data of all Er^{3+}-doped Y_2O_3 materials are shown in figure 1.

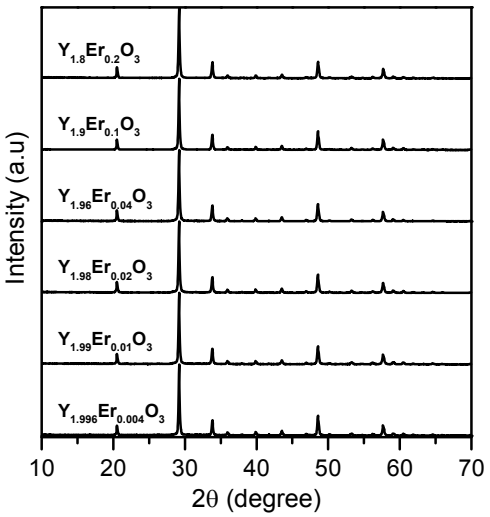

Figure 1. Powder XRD patterns of Er^{3+}-doped Y_2O_3 with various doping concentrations (0.2% to 10%) after annealing at 1000 °C for 2 hours.

EDX spectra were taken for three of the selected samples (0.2%, 5% and 10% Er^{3+}-doped Y_2O_3) and the concentrations of erbium and yttrium were measured to be those of the nominal values. EDX data is shown in the SI.

Lifetime measurements

Er^{3+}-doped Y_2O_3 powder yields a wide range of light emission, with discrete bands ranging from the visible (~520 nm) to the infrared (~1535 nm) following the blue excitation at room temperature. In addition, laser illumination at 980 nm is able to excite the visible bands through UC processes. The bands, shown in figure 2(a) and 2(c) for 0.2% Er^{3+}-doped Y_2O_3, can be assigned to the corresponding emissions from the $^4S_{3/2}$, $^4F_{9/2}$, $^4I_{11/2}$ and $^4I_{13/2}$ states to the ground $^4I_{15/2}$ state.

As we have stated in the introduction, spectral information is not, by itself, sufficient to understand the difference between DC and UC processes as it only provides a partial picture. In order to fully understand the occurring processes, it is necessary to obtain the details of the decay curves of all intervening states showing how each state is populated and depopulated. To quantify the decay constants, all the decay curves, I(t), were fitted with a double exponential equation,

$$I(t) = A_1 * \exp(-\frac{t}{\tau_1}) + A_2 * \exp(-\frac{t}{\tau_2}) \qquad (1)$$

Where I(t) is the decaying intensity at the maximum of the emission band, A_1, A_2 are the exponential pre-factors and τ_1 and τ_2 are the fitted decay times. This model is usually employed to account for the decay of erbium ions in an inhomogeneous environment, for example where ions are either in the bulk or near the surface and undergoing different quenching or energy transfer routes or when a population of the ions is close to the presence of impurities. Hence, it is widely phenomenologically employed without associated hypotheses on the nature of the parameters. The average decay time constant τ_{av} can be determined using [16],

$$\tau_{av} = \frac{A_1\tau_1^2 + A_2\tau_2^2}{A_1\tau_1 + A_2\tau_2} \qquad (2)$$

When the fit is good (and thus all processes are correctly phenomenologically accounted for), this is equivalent to taking a non-fitted average decay constant, calculated directly from the time dependence of the decaying intensity [39],

$$\tau_{av} = \frac{\int_0^\infty tI(t)dt}{\int_0^\infty I(t)dt} \qquad (3)$$

Figure 2(b) shows the recorded decay curves and corresponding fits of the $^4S_{3/2}$, $^4F_{9/2}$, $^4I_{11/2}$ and $^4I_{13/2}$ states for the 0.2% Er^{3+}-doped Y_2O_3 sample. The $^4S_{3/2}$ and $^4F_{9/2}$ emitting states (green and red emissions, respectively) show relatively short average DC lifetimes, τ_{av} < 120 µs, while the IR emitting states, $^4I_{11/2}$ and $^4I_{13/2}$, present lifetimes more than ten times longer, in the order of milliseconds. These long-lived $^4I_{11/2}$ and $^4I_{13/2}$ states can, in principle, act as intermediate states for further excitation under 980 nm excitation or participate in energy transfer processes between close erbium ions, causing the visible UC (figure 2c).

In the given excitation conditions, 0.2% Er^{3+}-doped Y_2O_3 shows the longest DC lifetimes along the $Y_{2-x}Er_xO_3$ series for all the emitting states; this is caused by the reduced non-radiative mechanisms for this dilution and particularly the small contribution of concentration-derived quenching such as CR [16-17]. The fact that the average UC decay time (~ 150 µs) is similar to the DC average lifetime (~ 120 µs) proves that energy transfer UC (ETU) is extremely restricted (figures 2b and 2d). In the general case, if the UC is only due to ESA, the $^4F_{7/2}$ emitting level is populated through the energy resonant $^4I_{11/2} + h\upsilon \rightarrow {}^4F_{7/2}$ process and the subsequent rapid relaxation to the green emitting levels ($^2H_{11/2}$ and $^4S_{3/2}$); therefore, the emission processes are exactly the same as under 488 nm excitation [25]. Figure 3, shows a much more significant difference between UC and DC average decay times for Er^{3+} concentrations higher than 0.5% (see SI for lifetime fitting and τ_{av} numbers). For these concentrations, the average lifetimes of $^4S_{3/2}$ and $^4F_{9/2}$ emitting states under 980 nm excitation are in the order of hundreds of microseconds, while the DC lifetimes are considerably shorter. These much higher values and differences constitute a direct evidence that the dominant UC mechanism under 980 nm excitation for high erbium concentrations is ETU involving the long lived $^4I_{11/2}$ and/or $^4I_{13/2}$ states as excitation reservoirs. ETU processes imply a modulation of the emission lifetime by the long-lived states acting as a reservoir [21, 23, 25, 40], as we discuss below. Importantly, the occurrence of ETU means that erbium-erbium interactions are present even at 0.5% Er^{3+} content.

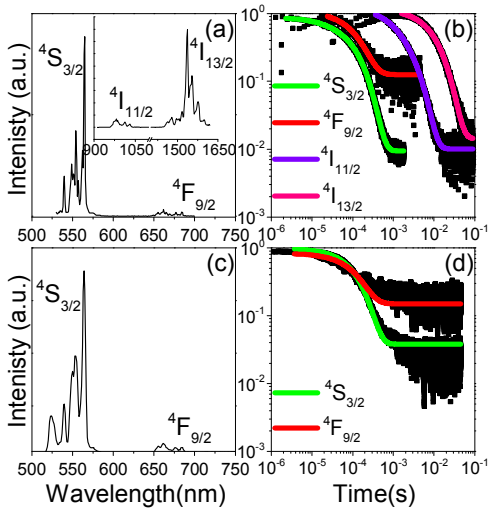

Figure 2. (a) Spectra of 0.2% Er^{3+}-doped Y_2O_3 under 488 nm excitation, (b) I(t) curves of all emitting states of 0.2% Er^{3+}-doped Y_2O_3 under 488 nm excitation, (c) Spectra of 0.2% Er^{3+}-doped Y_2O_3 under 980 nm excitation, (d) I(t) curves of all visible emitting states of 0.2% Er^{3+}-doped Y_2O_3 under 980 nm excitation.

In the case of 0.2% Er^{3+}-doped Y_2O_3, it is noteworthy that the green to red emission ratio is also very similar in the case of UC and DC spectra (figures 2a and 2c). This difference between UC and DC spectra is much more significant for the higher concentrations (see below).

Figure 3 summarizes the average lifetimes for the Er^{3+}-doped Y_2O_3 series when varying the doping concentration from 0.2, to 10 % for both the UC (excitation at 980 nm) and DC (pulsed excitation at 488 nm). Importantly, before discussing the average lifetime dependence of the emissions with the Er^{3+} concentration we must note here that the DC and UC time-resolved I(t) curves were measured with different excitation lasers: a pulsed 488 nm laser allowing for the measurement of the intrinsic population and depopulation for DC and a 980 nm CW laser, needed to achieve detectable UC, respectively, see above for power conditions. The different absorbed powers cause a completely different distribution of the population of the excited states. In order to study the effect of the excitation pulse length in the difference between DC and UC dynamics we also

measured the I(t) decay curves for the DC with different excitation pulse lengths by employing a modulated 405 nm CW laser and varying the laser power for the 488 nm laser pulse for the most diluted and most concentrated samples. The average decay times measured for 50 µs and 50 ms, 405 nm excitation pulses on 0.2% and 10% Er^{3+}-doped Y_2O_3 are also included in Figure 3. We observe in the figure that for all DC emission wavelengths the average lifetimes for the 0.2% Er^{3+}-doped Y_2O_3 are irrespective of the laser pulse length. This is also an evidence of the absence of energy transfer, as we will comment later. The lifetimes of the longer-lived IR emissions also show no dependence with the excitation length in the case of the 10% Er^{3+}-doped Y_2O_3. The green emission, however, shows an increased average lifetime for the 405 nm, 50 µs excitation pulses, which is almost an order of magnitude higher with respect to the 488 nm, 7 ns excitation, and reaches up to two orders of magnitude higher value for the 405 nm, 50 ms excitation. The red emission shows a decrease in the lifetime for the 50 µs long excitation, approximating the green emission lifetime, but experiences an increase for the 50 ms excitation, taking almost the same value as for UC (see table S2 in the SI for numerical values). Interestingly, 405 nm, 500 µs pulse duration excitation provides an intermediate value of 76 µs for the $^4F_{9/2}$ DC emission, close to the 65 µs reached for 488 nm pulsed excitation. A similar dependence with the laser power has been observed upon varying the energy of the OPO laser pulses (see table S3, SI).

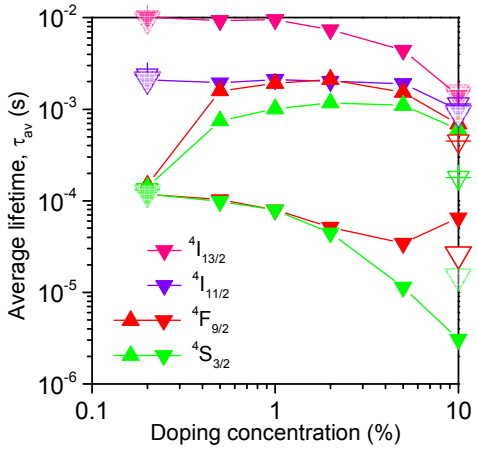

Figure 3. Average decay lifetime of all emitting states of the Er^{3+}-doped Y_2O_3 studied samples for DC and UC processes (see text for excitation conditions). Up-triangles: UC, down-triangles: DC, open symbols: excitation for a 50 µs long pulse, crossed symbols: 50 ms pulse, pink symbols: emission from $^4I_{13/2}$, violet symbols: emission from $^4I_{11/2}$, red colour symbols: emission from $^4F_{9/2}$, green colour symbols: emission from thermalized $^4S_{3/2}$.

Figure 3 shows that the average DC lifetimes of the $^4I_{13/2} \rightarrow {}^4I_{15/2}$ and $^4I_{11/2} \rightarrow {}^4I_{15/2}$ transitions experience a monotonous lifetime decrease when increasing the erbium concentration. This can be explained in terms of concentration dependent non-radiative theory [16]. Concentration dependent non-radiative decays occur due to the enhancement of energy transfer processes, which include excitation hopping (and may lead the excitation to non-radiative traps) and CR mechanisms involving the emitting levels, both becoming more likely as the average distance between Er^{3+} ions is reduced. Some of the CR mechanisms (which may be resonant or vibrationally assisted) include the cooperative non-radiative decays $[^4I_{11/2}, {}^4I_{11/2}] \rightarrow [^4F_{7/2}, {}^4I_{15/2}]$, $[^4I_{13/2}, {}^4I_{11/2}] \rightarrow [^4F_{9/2}, {}^4I_{15/2}]$, $[^4I_{11/2}, {}^4I_{13/2}] \rightarrow [^4F_{9/2}, {}^4I_{15/2}]$ and $[^4I_{13/2}, {}^4I_{13/2}] \rightarrow [^4I_{9/2}, {}^4I_{15/2}]$ (and maybe $[^4I_{9/2}, {}^4I_{11/2}] \rightarrow [^4I_{13/2}, {}^4F_{9/2}]$ [14,21] and $[^4F_{7/2}, {}^4I_{11/2}] \rightarrow [^4F_{9/2}, {}^4F_{9/2}]$ [24]) as represented in figure 4 (ETU1, ETU2, $CR7^{(L2)}$, $CR8^{(L3)}$, $CR6^{(L1)}$ and CR1, respectively) . In fact, the first two of these processes contribute directly to the ETU and thus are labelled correspondingly).

Figure 3 also shows that under 980 nm excitation (UC regime), the lifetimes of the $^4S_{3/2}$ and $^4F_{9/2}$ emitting states show a similar trend. They both increase as the doping concentration increases from 0.2% to 2%. At higher doping concentrations there is a subsequent decrease in the lifetime. This variation emphasizes that the dynamics of the reservoir and transfer govern the decay of the UC emission [23, 25]. Interestingly, figure 3 shows that the UC lifetime of the $^4F_{9/2}$ (red) emitting state in the intermediate concentration regime 0.5-5% is considerably longer (approximately twice as long) than that of $^4S_{3/2}$ emitting state. However, the DC lifetime measured under 488 nm excitation is almost the same in the case of erbium dilutions below 2%. Thus, it can be concluded that there are different energy transfer processes populating the $^4S_{3/2}$ and $^4F_{9/2}$ emitting states, respectively. According to established understanding the longer average lifetime for the red emission suggests that the states feeding $^4F_{9/2}$ are correspondingly longer-lived than those for the green emission, implying that the energy transfer, $[^4I_{13/2}, {}^4I_{11/2}] \rightarrow [^4F_{9/2}, {}^4I_{15/2}]$ (ETU2) or the reciprocal, $[^4I_{11/2}, {}^4I_{13/2}] \rightarrow [^4F_{9/2}, {}^4I_{15/2}]$ ($CR7^{(L2)}$) are relevant in ETU in the concentrated systems of the studied series (see supplementary information Table S4, for a discussion and, for instance, [21, 28]). The fact that the concentration at which these processes appear is as low as 6.71×10^{19} Er^{3+} ions / cm^3 has critical consequences.

Moreover, the concentration enhanced incidence of these CR routes in the re-population of the $^4F_{9/2}$ even in the DC regime (together with the other looping CR mechanism $[^4I_{13/2}, {}^4I_{13/2}] \rightarrow [^4I_{9/2}, {}^4I_{15/2}]$ ($CR8^{(L3)}$, as given in figure 4) [19, 36, 38, 41]), which repopulate the red emitting state and the $^4I_{9/2}$ reservoir, respectively via long-lived $^4I_{13/2}$ state), explains the increase of the red DC emission lifetime observed in the high concentration Er^{3+}-doped Y_2O_3 when the population of the $^4I_{11/2}$ and $^4I_{13/2}$ states is large (figure 3). This model has implications in the changes of the red to green emission colour ratios as a function of power, concentration and excitation wavelength (DC or UC). Importantly, both the indistinguishable (in the excitation conditions) ETU2/$CR7^{(L2)}$ and $CR8^{(L3)}$ looping require a population

of the lowest lying states via multiphonon, radiative or other CR decays (see figure 4 for a global picture and figure S9/Table S4 in the SI for an approximate description and discussion).

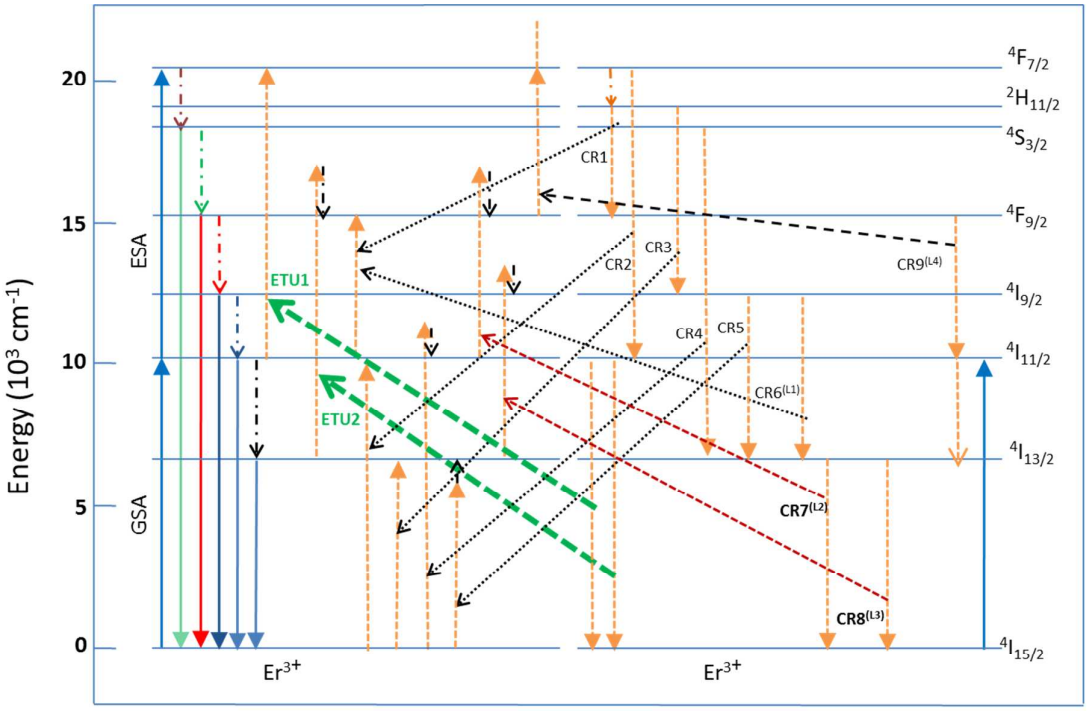

Figure 4. Simplified energy level diagram and most relevant radiative and energy transfer mechanisms in Er^{3+}-doped Y_2O_3. Ground state absorption (GSA), excited state absorption (ESA), green, red and IR luminescence, and energy transfer UC (ETU) as well as cross relaxations (CR) are presented. See SI for a deeper consideration and argumentation of the most relevant ones and a set of dynamic equations ruling the time evolution of the populations.

The lifetime study can be summarized as follows: (1), the IR emitting states $^4I_{11/2}$ and $^4I_{13/2}$ experience a systematic lifetime decrease with increasing doping concentration, which we assign to conventional concentration quenching (i.e. hopping and CR). This quenching gets more severe as the concentration increases and has important implications in the visible photoluminescence, as this levels act as excitation reservoirs due to their long lifetime, in the order of milliseconds. (2), under 980 nm excitation, the lifetime increases from 0.2% to 2% and then decreases from 2% to 10%. The first increase is due to the UC route change from a situation in which ESA is the main mechanism to a prevalence of ETU involving the well-known [$^4I_{11/2}$, $^4I_{11/2}$] → [$^4F_{7/2}$, $^4I_{15/2}$] (ETU1) and, since the lifetime of the red emission is approximately double than that of the green emission, ETU2 ([$^4I_{13/2}$, $^4I_{11/2}$] → [$^4F_{9/2}$, $^4I_{15/2}$])/CR7$^{(L2)}$ [$^4I_{11/2}$, $^4I_{13/2}$] → [$^4F_{9/2}$, $^4I_{15/2}$] [21, 23]. The subsequent decrease with increasing erbium concentration is predominantly caused by the severe concentration quenching CRi (i = 1-8) which cause a decay in the intrinsic lifetime not only of the emitting levels but, also for the $^4I_{13/2}$, $^4I_{11/2}$ excitation reservoir states in the E < 11 000 cm^{-1} (~1.35 eV) region caused by CRi (i > 5) [particularly for Er^{3+} higher than 1%,], see SI. Interestingly, CRi (i < 5) cause a decrease in the green lifetime, and should be active for both DC and UC, but in the 1 to 8 range no CRi depopulates $^4F_{9/2}$. Sure this kind of mechanisms exist, as the DC lifetime tends to decrease too in the 0.2 - 5% concentration range; hence, it is likely that the opposite to CR1, which we label CR9^{L4} plays a role plus maybe other less resonant CRs from $^4F_{9/2}$ to higher lying levels.

Importantly, looping mechanisms ETU2, CR7$^{(L2)}$, CR8$^{(L3)}$ and CR6$^{(L1)}$ that re-populate the upper excited states for high concentrations and high powers for both the UC and DC regimes [18, 19, 21, 23, 38, 41] get enhanced when the Er^{3+} concentration is increased. The severe enhancement of these processes that (except CR6$^{(L1)}$) rely on long-lived lower lying reservoirs explains the increase of the red emission life when the laser energy increases.

Difference between up-conversion and down-conversion spectra

The emission spectra under 488 nm and 980 nm excitations are shown in figure 5(a). The green to red ratio decreases with increasing erbium concentration under both 488 nm and 980 nm excitations, but follows a different trend as showed in figure 5(b). Under 488 nm OPO excitation (DC), the green to red ratio change is

small from 0.2% to 1% erbium doping concentration, while it decreases a factor 10 from 1% to 10% erbium doping concentration. However, for the 980 nm excitation, it decreases considerably more over the 0.2% to 1% concentration range with comparatively little subsequent change. Our estimations of temperature differences caused by different excitation conditions and their effect on the emission properties for the different samples show that concentration effects are dominant and must be taken into account to explain this evolution.

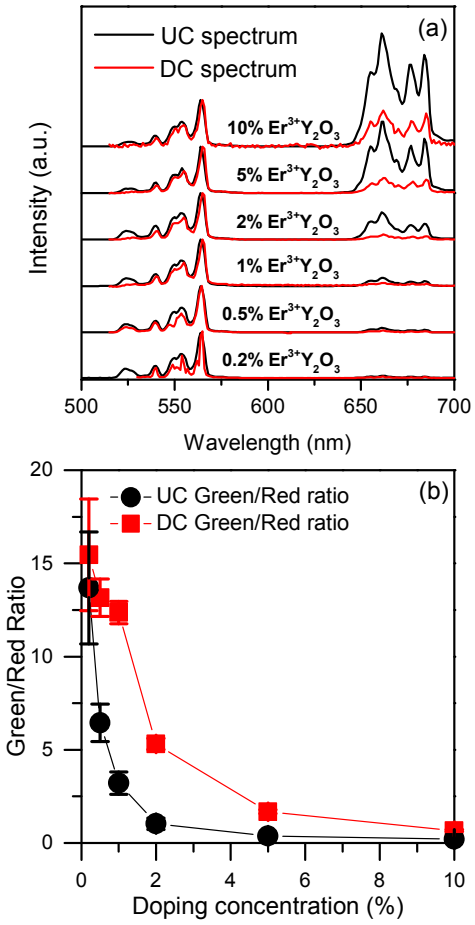

Figure 5. (a) Spectra under both 980 nm (UC) and 488 nm (DC) excitations; (b) Green to red ratio change with doping concentration for UC and DC processes.

Concentration-induced processes, which affect the population (and decay) of $^4S_{3/2}$ and $^4F_{9/2}$ states differently, explain the change in the DC and UC spectra in the explored power regime. Upon direct excitation on the $^4F_{7/2}$ state, the CR-induced changes in the population are not significant from 0.2 % to 1% and, as observed in figure 3, neither are the decay processes, as the lifetime is similar for both the red and the green emissions (figure S3, SI). From 2 % to 10 %, as concentration quenching becomes significant and a severe CR including the processes CRi ($i < 5$) and the looping mechanisms CRi^L ($9 > i > 6$) for high populations of the IR states start to occur, causing that the red emission becomes comparatively more intense than the green one, and the lifetime gets increased for given power or excitation length conditions.

The change in the UC routes explains the change in the emission spectra for the 980 nm excitation UC regime. At 0.2% doping concentration, ESA is the significant UC route, the spectrum being very similar to that observed under 488 nm excitation. With increasing erbium concentration, ETU gets more preponderant. The ETU1 process $[^4I_{11/2}, {}^4I_{11/2}] \rightarrow [^4F_{7/2}, {}^4I_{15/2}]$ contributes to populate the upper states as the ESA or similarly to the DC regime, but ETU2 $[^4I_{11/2}, {}^4I_{13/2}] \rightarrow [^4F_{9/2}, {}^4I_{15/2}]$ / $CR7^{(L2)}$ $[^4I_{11/2}, {}^4I_{13/2}] \rightarrow [^4F_{9/2}, {}^4I_{15/2}]$ and the other CR and looping mechanisms described above and, result in a higher nominal population of $^4F_{9/2}$. Thus, there is a steady increase of red emission with increasing concentration from 0.2% to 10%. The considerable increase in the population of the long-lived lower-lying $E < 11000$ cm^{-1} (~ 1.35 eV) states causes that this decrease is comparatively higher than in DC in the 0.5- 2% range.

Conclusions

We have studied the UC mechanisms in the simple Er^{3+}-doped Y_2O_3 system as a function of the Er^{3+} concentration through the change in the dynamics of the emitting states, including the $^4I_{11/2}$ and $^4I_{13/2}$ states. We have done this by employing different excitation powers, pulse lengths and wavelengths. We have described the progressive importance of energy transfer and CR as the Er^{3+} content increases from 0.2% to 10% and its implications in the spectral properties and decay times of the UC (excitation at 980 nm) but also for DC. These processes, including looping mechanisms result in an increase of the DC decay time for high Er^{3+} concentration in given excitation powers. Moreover ETU/CR from $^4I_{11/2}$ to $^4I_{11/2}$ and $^4I_{13/2}$ cause a dominance of the population of the red emitting state for UC at high Er^{3+} concentrations, thus affecting severely the green to red emission ratio and also have an influence in the UC lifetimes of the green and red emissions [21]. Importantly these processes start being significant at concentrations as low as 6.71×10^{19} Er^{3+} ions / cm^3.

The consideration of these ET and CR routes must be taken into account for understanding of the doping concentration dependent UC and DC properties of this material (and maybe others) and subsequent implementation of tailored emitting colour properties for phosphors, display and biological applications. These results could also make more accessible a deeper insight into more complex, but more practical Er^{3+}/Yb^{3+} co-doped systems.

Acknowledgement:

The authors thank Dr. R. Wilson for XRD measurements and Dr. Z. Luklinska for EDX measurements. HL is funded by the China Scholarship Council and Queen Mary University of London. IH acknowledges funding from the EU FP7 (Marie Curie-CIG-Grant 303535).

References:

1 V. V. Ovsyankin and P. P. Feofilov, *JETP Lett.*, 1966, **4**, 317.
2 F. Auzel, *Chem. Rev.*, 2004, **104**, 139.
3 F. Vetrone, J. C. Boyer, J. A. Capobianco, *In the Encyclopedia of Nanoscience and Nanotechnology*, 2004, **10**, 725.
4 X. Liu, H. Qian, Y. Ji, Z. Li, Y. Shao, Y. Hu, G. Tong, L. Li, W. Guo and H. Guo, *RSC Adv.*, 2012, **2**, 12263.
5 E. Downing, L. Hesselink, J. Ralston, R. Macfarlane, *Science*, 1996, **273**, 1185.
6 J. Zhao, D. Jin, E. P. Schartner, Y. Lu, Y. Liu, A. V. Zvyagin, L. Zhang, J. M. Dawes, P. Xi, J. A. Piper, E. M. Goldys and T. M. Monro, *Nature Nanotechnology*, 2013, **8**, 729.
7 M. Kong, W. Hu, F. Cheng, Z. Huang, J. Zhang, Z. Han, N. Shi, Q. Fan, S. Chen and W. Huang, *J. Mater. Chem. C.*, 2013, **1**, 5872.
8 R. Martín-Rodríguez, S. Fischer, A. Ivaturi, B. Froehlich, K. W. Krämer, J. C. Goldschmidt, B. S. Richards and A. Meijerink, *Chem. Mater.*, 2013, **25**, 1912.
9 K. W. Krämer, D. Biner, G. Frei, H. U. Güdel, M. P. Hehlen, and S. R. Lüthi, *Chem. Mater.,* 2004, **16**, 1244.
10 S. Heer, K. Kömpe, H. U. Güdel, and M. Haase, *Adv. Mater.,* 2004, **16**, 2102.
11 F. Wang, Y. Han, C. S. Lim, Y. Lu, J. Wang, J. Xu, H. Chen, C. Zhang, M. Hong and X. Liu, *Nature*, 2010, **463**, 1061.
12 J. Wang, H. Song, W. Xu, B. Dong, S. Xu, B. Chen, W. Yu and S. Zhang, *Nanoscale*, 2013, **5**, 3412.
13 J. Zhao, Z. Lu, Y. Yin, C. McRae, J. A. Piper, J. M. Dawes, D. Jin and E. M. Goldys, *Nanoscale*, 2013, **5**, 944.
14 H. X. Mai, Y. W. Zhang, L. D. Sun and C. H. Yan, *J. Phys. Chem. C.*, 2007, **111**, 13721.
15 R. B. Anderson, S. J. Smith, P. Stanley May and M. T. Berry, *J. Phys. Chem. Lett.*, 2014, **5**, 36.
16 M. C. Tan, G. A. Kumar, R. E. Riman, M. G. Brik, E. Brown and U. Hommerich, *J. Appl. Phys.*, 2009, **106**, 063118.
17 J. W. Stouwdam and F. C. J. M. van Veggel, *Nano Lett.*, 2002, **2**, 733.
18 S. Sivakumar, F. C. J. M. van Veggel, P. Stanley May, *J. Am. Chem. Soc.*, 2007, **129**, 620 .
19 P. S. Golding, S. D. Jackson, T. A. King and M. Pollnau, *Phys. Rev. B.*, 2000, **62**, 856.
20 J. Qiu, P. G. Kazanski, J. Si, K. Miura, T. Mitsuyu, K. Hirao and A. L. Gaeta, *Appl. Phys. Lett.*, 2000, **77**, 1940.
21 R. Balda, A. J. Garcia-Adeva, J. Fernández and J. M. Fdez-Navarro, *J. Opt. Soc. Am. B.*, 2004, **21**, 744.
22 J. A. Capobianco, F. Vetrone, T. D´Alesio, G. Tessari, A. Speghini and M. Bettinelli, *Phys. Chem. Chem. Phys.*, 2000, **2**, 3203.
23 J. A. Capobianco, F. Vetrone and J. C. Boyer, *J. Phys. Chem. B.*, 2002, **106**, 1181.
24 F. Vetrone, J. C. Boyer, J. A. Capobianco, A. Speghini and M. Bettinelli, *Chem. Mater.,* 2003, **15**, 2737.
25 I. Etchart, A. Huignard, M. Bérard, M. N. Nordin, I. Hernández, R. J. Curry, W. P. Gillin and A. K. Cheetham, *J. Mater. Chem.*, 2010, **20**, 3989.
26 E. De la Rosa-Cruz, L. A. Díaz-Torres, R. A. Rodríguez-Rojas, M. A. Meneses-Nava and O. Barbosa-García, *Appl. Phys. Lett.*, 2003, **83**, 4903.
27 H. Eilers, *Materials Letters*, 2006, **60**, 214.
28 L. Agazzi, K. Wörhoff, A. Kahn, M. Fechner, G. Huber and M. Pollnau, *J. Opt. Soc. Am. B.,* 2013, **30**, 663.
29 H. Guo, W. Zhang, L. Lou, A. Brioude and J. Mugnier, *Thin Solid Films*, 2004, **458**, 274.
30 J. Silver, M. I. Martinez-Rubio, T. G. Ireland, G. R. Fern and R. Withnall, *J. Phys. Chem. B.*, 2001, **105**, 948.
31 Y. Mao, T. Tran, X. Guo, J. Y. Huang, C. Ken Shih, K. L. Wang and J. P. Chang, *Adv. Funct. Mater.,* 2009, **19**, 748.
32 J. Zhang, S. Wang, T. Rong and L. Chen, *J. Am. Ceram. Soc.*, 2004, **87**, 1072
33 G. Y. Chen, H. C. Liu, G. Somesfalean, Y. Q. Sheng, H. J. Liang, Z. G. Zhang, Q. Sun and F. P. Wang, *Appl. Phys. Lett.*, 2008, **92**, 113114.
34 H. Guo and Y. M. Qiao, *Optical Materials*, 2009, **31**, 583.
35 F. Hanic, M. Hartmanová, G. G. Knab, A. A. Urusovskaya and K. S. Bagdasarov, *Acta Cryst.*, 1984, **B40**, 76.
36 L. Agazzi, K. Wörhoff and M. Pollnau, *J. Phys. Chem. C.*, 2013, **117**, 6759.
37 J. F. Suyver, A. Aebischer, S. García-Revilla, P. Gerner and H. U. Güdel, *Phys. Rev. B.*, 2005, **71**, 125123.
38 C. Renero-Lecuna, R. Martín-Rodríguez, R. Valiente, J. González, F. Rodríguez, K. W. Krämer and H. U. Güdel, *Chem. Mater.*, 2011, **23** 3442.
39 J. R. Lakowicz, *Principles of fluorescence of spectroscopy, 3rd edition,* 2006.
40 I. Etchart, I. Hernández, A. Huignard M. Bérard, W. P. Gillin, R. J. Curry and Anthony K. Cheetham, *J. Mater. Chem.*, 2011, **21**, 1387.
41 I. Hernández, R. H. C. Tan, J. M. Pearson, P. B. Wyatt and W. P. Gillin, *J. Phys. Chem. B.,* 2009, **113**, 7474.

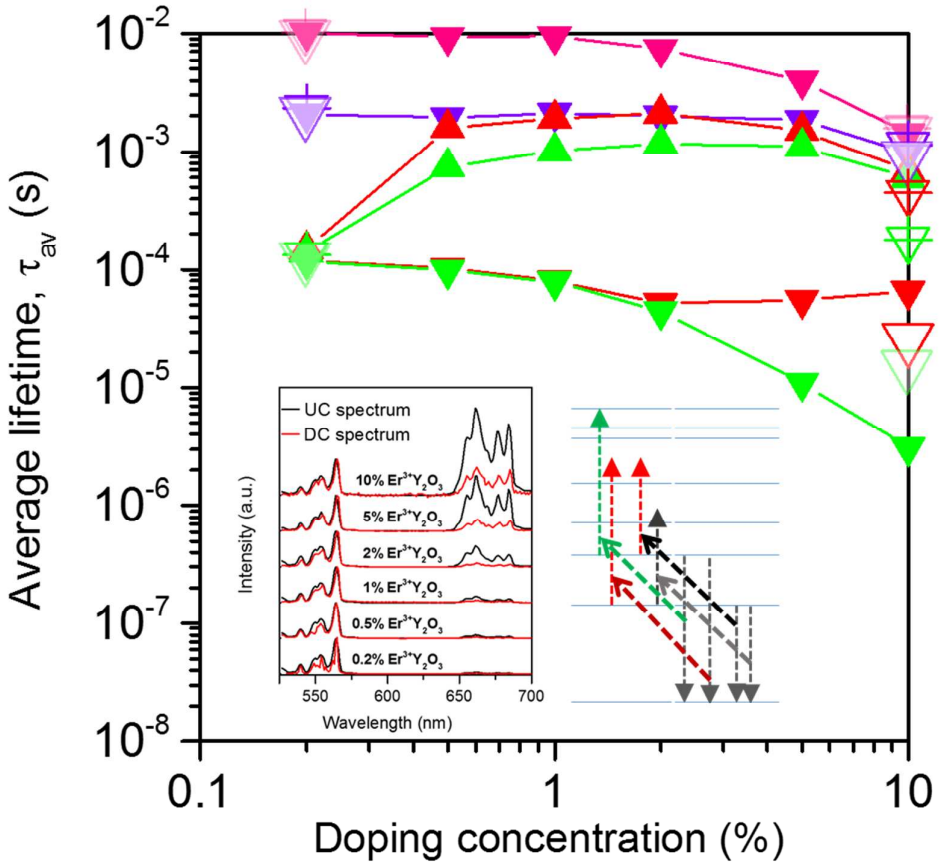

Er^{3+} energy transfer mechanisms and their influence in the dynamics and emission colours are considered for upconversion and downconversion regimes.